Ceramics

Effect of O/N content on the phase, morphology, and optical properties of titanium oxynitride thin films

Sharafat Ali[1], Roger Magnusson[1], Oleksandr Pshyk[2,3], Jens Birch[2], Per Eklund[2], and Arnaud le Febvrier[2,*] (iD)

[1] School of Engineering, Department of Built Environment and Energy Technology, Linnaeus University, 351 95 Växjö, Sweden
[2] Department of Physics, Chemistry and Biology (IFM), Linköping University, 58183 Linköping, Sweden
[3] Present address: Empa—Swiss Federal Laboratories for Materials Science and Technology, 8600 Dübendorf, Switzerland

ABSTRACT

Phase formation, morphology, and optical properties of Ti(O,N) thin films with varied oxygen-to- nitrogen ration content were investigated. The films were deposited by magnetron sputtering at 500 °C on Si(100) and c-plane sapphire substrate. A competition between a NaCl B1 structure $TiN_{1-x}O_x$, a rhombohedral structure $Ti_2(O_{1-y}N_y)_3$, and an anatase structure $Ti(O_{1-z}N_z)_2$ phase was observed. While the N-rich films were composed of a NaCl B1 $TiN_{1-x}O_x$ phase, an increase of oxygen in the films yields the growth of rhombohedral $Ti_2(O_{1-y}N_y)_3$ phase and the oxygen-rich films are comprised of a mixture of the rhombohedral $Ti_2(O_{1-y}N_y)_3$ phase and anatase $Ti(O_{1-z}N_z)_2$ phase. The optical properties of the films were correlated to the phase composition and the observation of abrupt changes in terms of refractive index and absorption coefficient. The oxide film became relatively transparent in the visible range while the addition of nitrogen into films increases the absorption. The oxygen rich-samples have bandgap values below 3.75 eV, which is higher than the value for pure TiO_2, and lower than the optical bandgap of pure TiN. The optical properties characterizations revealed the possibility of adjusting the band gap and the absorption coefficient depending on the N-content, because of the phases constituting the films combined with anionic substitution.

🖄 Springer

Introduction

Transition-metal oxynitrides, such as Ti(O,N), are known for their optical and electronic properties, mechanical behavior, and chemical stability [1–5]. A large number of studies have been reported on the formation and properties of titanium oxynitride, Ti(O,N), where the properties of these materials strongly depend on their compositions, notably the O/N ratio. Ti(O,N) has been used in thin film resistors, solar selective collectors, biomaterials, hard coating, and decorative coatings [6–9].

Ti(O,N) thin films have been fabricated by various techniques including DC magnetron sputtering, RF magnetron sputtering, pulsed laser deposition, electron beam evaporation, ion-assisted deposition, and chemical vapor deposition [3, 10–14]. Magnetron sputtering is a common technique, thanks to its versatility and reliability to control the microstructure and composition of the Ti(O,N) films which allows to tune mechanical, electrical and optical properties of the films [8, 11, 15].

The Ti(O,N) materials system has a complex behavior between conductive TiN and insulating TiO_2 compounds [2]. Several stable phases can be found in the phase diagram Ti–O–N such as TiN, Ti_2N, Ti_2O_3, Ti_3O_5, TiO_2 (rutile or anatase) and TiO, where nitrogen and oxygen can substitute for each other [15, 16]. During the magnetron sputtering process, phase formation in the films depends on process parameters such as the energy of sputtered species, the amount of reactive gases, and substrate temperature. Martin et al. reported that the crystal structure of $Ti(O_n,N_m)$ films depends on oxygen/nitrogen content ($0 \leq n \leq 2.0$ and $0 \leq m \leq 1.0$) and changed from NaCl B1 TiN to anatase TiO_2 through intermediate phase (NaCl B1 TiN, anatase and rutile TiO_2, and the monoclinic Ti_3O_5) [17]. Others reported a change from crystalline NaCl B1 structure of Ti(O,N) to amorphous films when the oxygen content is increased during the deposition process [18].

The partial substitution of nitrogen for oxygen or vice versa (O/N ratio) in a disordered manner in the same structure impacts the bonding environment between the cations and anions, which affects the physical properties of the films. Another example of the effect of anionic substitution is the mechanical properties, e.g., hardness and Young's modulus, of Ti(ON) thin films was increased with increasing the

O/N ratio in the thin films [19–21]. The bulk moduli of NaCl-type structure $TiN_{1-x}O_x$ has been reported with decreasing of the mechanical performance when oxygen is inserted in the structure [19, 20]. The substitution of oxygen by nitrogen was the key for decreasing the bandgap energy of TiO_2 [22, 23]. Abhishek et al. have reported that of Ti based oxynitrides ($Ti_nN_2O_{2n-3}$) created by N substitution in Ti^{3+} oxides, had band gaps below 2.5 eV and band edge positions suitable for high efficiency photocatalytic or photovoltaic activity [22]. Nevertheless, there is still a need for further studies of refractive index and dielectric properties of Ti(O,N) films and compositions-structure-properties relations.

The present study is an investigation of the growth of Ti(O,N) films by RF magnetron reactive sputtering of Ti target at varied N/O gas flow ratio. The objective was to investigate the phase constitution, morphology, and optical properties of Ti(O,N) thin films as a function of N/O content in the films. Mueller Matrix Spectroscopic ellipsometry (MMSE) was employed to determine the optical properties, e.g., refractive index, extinction coefficient, band gap, and UV–vis absorption.

Material and methods

Ti(O,N) films were synthesized by RF magnetron reactive sputtering of Ti target in an ultrahigh vacuum (UHV; base pressure < 3 Pa $\times 10^{-7}$ Pa) deposition system described elsewhere [24]. Ti(O,N) thin films were deposited simultaneously on silicon (001) and sapphire (0001) (c-plane) substrates. Prior to introducing the substrates in the reaction chamber the substrates were cleaned ultrasonically in acetone and ethanol successively for 10 min each. A mixture of oxygen (O_2), nitrogen (N_2), and argon (Ar) gases was used. The total gas flow was kept constant at 40 sccm for a constant pressure of 0.38 Pa (2.8 mTorr), with Ar flow fixed at 27 sccm and reactive gas flow fixed at 20 sccm while $\%N_2$ in the reactive gas varied between 98 and 84% (Table 1). The Ar flow was kept at 27 sccm for all samples. All the samples were prepared with constant Ti target power of 100 W and a substrate temperature of 500 °C. Prior to each deposition, the Ti target was sputter-cleaned in Ar (27 sccm Ar / 0.26 Pa) for 5 min. The deposition time was 1 h.

Table 1 Deposition parameters used for the growth of Ti(O,N) films

Sample #	Ti target Power (W)	Argon flow (sccm)	Reactive gas flow (sccm)		
			O_2	N_2	$N_2/(N_2 + O_2)$
1	100	27	0.4	19.6	98%
2	100	27	1.2	18.8	94%
3	100	27	2.0	18.0	90%
4	100	27	2.4	17.6	88%
5	100	27	2.8	17.2	86%
6	100	27	3.2	16.8	84%

The structure and phase identification of the films were performed by X-ray diffraction (XRD) using a Panalytical X'pert PRO MPD diffractometer equipped with a X'celerator detector and CuKα radiation operated at 45 kV and 40 mA. The XRD patterns were recorded with identical settings. The surface morphology of the films on sapphire and silicon substrates were investigated by scanning electron microscope (ZEISS Gemini SEM 650) operated with an acceleration voltage of 2.00 kV and in-lens detector was used to observe the surface morphology.

The elemental composition and chemical bonding environment of the thin films deposited on sapphire and Si substrates were studied by X-ray photoelectron spectroscopy (XPS). The analyses were performed by an Axis Ultra DLD instrument from Kratos Analytical (UK) with a monochromatic Al Kα radiation (hν = 1486.6 eV). All the samples were sputter-etched to remove surface contamination, which can interfere with the accuracy of the XPS measurements. All films are sputter-etched with a 4.0 keV Ar$^+$ ion beam incident at an angle of 70° with respect to the surface normal. The Ar$^+$ ion energy is then reduced to 0.5 keV for 600 s to minimize surface damage at the last measurement step. A charge neutralizer was used when necessary due to possible poor electrical conductivity of the sample. The analyzed area has a size of 0.3×0.7 mm^2 and is centered in the middle of the 3×3 mm^2 etched area. Elemental concentrations were determined with CasaXPS software employing Shirley-type background [25] and the manufacturer's sensitivity factors. Preferential sputtering of the nitrogen and oxygen species is also taken into consideration [26], thus resulting a 3% error bar in the quantitative measurements. The binding energy scale is calibrated using the ISO-certified procedure [27]. Charge referencing is done by setting the Fermi edge of the films

at 0 eV when the charge neutralized was not used [28].

The optical properties of the Ti(O,N) thin films were examined using Mueller matrix spectroscopic ellipsometry (MMSE). Reflection measurements were conducted using a dual rotating compensator ellipsometer (RC2®) from J.A.Woollam Co., Inc. at three different angles of incidence (45°, 55° and 65°). The ellipsometry data were analyzed using the CompleteEASE software (version 6.63), also from J.A.Woollam Co., Inc. The data were fitted to models consisting of combinations of Cody-Lorentz oscillators [29] and Drude oscillators [30] in order to find the complex refractive index of the Ti(O,N) films. Five films (two on Si substrate e.g., $TiO_{1.06}N_0.60$, and $TiO_{1.67}N_{0.14}$, and three on sapphire substrate e.g., $TiO_{0.89}N_{0.71}$, $TiO_{1.27}N_{0.49}$, and $TiO_{1.83}N_{0.08}$) required modeling with a gradient in the refractive index, indicating a variation of density or grain size towards the surface of the film. Details about modelling can be found in Table S1 in supplementary information. Database values from the software were used to represent the optical properties of the sapphire and silicon, including a native oxide, substrates.

Results and discussion

The elemental compositions of the Ti(O,N) thin films determined by XPS are presented in Table 2. For the reason of convenience, the composition was normalized for Ti = 1, and the thin films are categorized progressively by decreasing N content in the thin films. The N content in the thin films gradually decreased from ≈ 37 at.% to ≈ 3 at.% while the O content increased from ≈ 25 at.% to ≈ 62 at.%. The thin films composition changed from N-rich $TiO_{0.73}N_{0.84}$ to O-rich $TiO_{1.67}N_{0.14}$ on Si substrate and between $TiO_{0.63}N_{0.96}$ and $TiO_{1.83}N_{0.08}$ on c-plane

Table 2 Composition of the films analyzed by XPS

Sample #	Analysis elemental composition (at.%) ± 1.5%			Composition normalized with Ti = 1	
	Ti	N	O	TiO_xN_y	Ti(O,N)
Si					
1	38.9	32.6	28.5	$TiO_{0.73}N_{0.84}$	$Ti(O,N)_{1.57}$
2	36.6	26.1	37.3	$TiO_{1.02}N_{0.71}$	$Ti(O,N)_{1.74}$
3	37.6	22.6	39.8	$TiO_{1.06}N_{0.60}$	$Ti(O,N)_{1.66}$
4	36.3	15.5	48.3	$TiO_{1.33}N_{0.43}$	$Ti(O,N)_{1.76}$
5	36.3	8.6	55.2	$TiO_{1.52}N_{0.24}$	$Ti(O,N)_{1.76}$
6	35.6	4.9	59.5	$TiO_{1.67}N_{0.14}$	$Ti(O,N)_{1.81}$
c-plane Al_2O_3					
1	38.7	37.1	24.2	$TiO_{0.63}N_{0.96}$	$Ti(O,N)_{1.58}$
2	38.4	27.4	34.3	$TiO_{0.89}N_{0.71}$	$Ti(O,N)_{1.61}$
3	36.3	17.7	46.0	$TiO_{1.27}N_{0.49}$	$Ti(O,N)_{1.75}$
4	36.0	11.3	52.7	$TiO_{1.47}N_{0.31}$	$Ti(O,N)_{1.78}$
5	36.4	7.9	55.7	$TiO_{1.53}N_{0.22}$	$Ti(O,N)_{1.75}$
6	34.3	2.8	62.9	$TiO_{1.83}N_{0.08}$	$Ti(O,N)_{1.92}$

Al_2O_3 substrate. A similar trend was also observed by Banakh et al.[31]. This observation is consistent with the deposition conditions where the N_2/O_2 gas flow ratio was varied. Furthermore, a few percent of O_2 (2% of flow ratio) were enough for the formation of film containing 24—29% of oxygen ($TiO_{0.73}N_{0.84}$), which is expected because the affinity of oxygen for titanium is much higher than that of nitrogen. This behavior is typical for both metal containing oxynitride thin films [32–34], and bulk oxynitride glasses [35–37]. The relative anion/cation ratio in Ti(O,N), increased from ≈ 1.6 to ≈ 1.9 with increasing the O_2 flow which is close to the relative anion/cation ratio of Ti_2O_3 (1.5) and in between the relative anion/cation ratio of TiN (1.0) and TiO_2 (2.0).

Figure 1 shows XRD patterns of Ti(O,N) films with varied O/N composition on Si substrate and c-plane sapphire substrates for. On Si substrate, except the substrate peaks situated at 32.9° and 69.1°, few weak diffractions peaks can be observed throughout the series. The XRD peak situated around 25° was identified as a a-TiO_2 structure (anatase (ICDD 00–021-1272)) for high oxygen containing film. The peak situated around 44° can be identified as a NaCl B1 structure, similar to TiN (ICDD 00–038-1420), or rhombohedral r-Ti_2O_3 structure (ICDD 00–008-0117) for middle-high nitrogen containing films, respectively. The series can be divided into two subgroups: (i) two films with the highest nitrogen content and (ii) the four additional films in the series with the highest oxygen content for which a XRD peak from a-TiO_2 structure emerged from the background.

On c-plane sapphire, the features are more pronounced. The substrate peaks are situated at 20.5°, 40.6° and 64.5°. With a higher N content, the XRD pattern presents one diffraction peak at $2\theta = 36.6°$ and can be identified as the 111 peak of a NaCl structure or as the 0006 reflection from a rhombohedral Ti_2O_3 structure. The anionic substitution is possible for both material yielding to B1-$TiN_{1-x}O_x$ and r-$Ti_2(O_{1-y}N_y)_3$ oxynitride phases yielding a variation of cell parameter [5, 23, 38]. The (0001) preferential film orientation of r-$Ti_2(O_{1-y}N_y)_3$ could be resulting from similarities of crystallographic structure between the substrate (space group: R-3c, a = 4.85 Å, c = 13.27 Å, ICDD 01–071-1684) and the film (space group: R-3c, a = 5.13 Å, c = 13.66 Å, ICDD 00–008-0117), while the (111) preferential film orientation of NaCl B1 $TiN_{1-x}O_x$ is often observed for a NaCl structure material grown on c-plane sapphire [39, 40].

The abrupt change of the intensity and broadening of the peaks at ~ 81° was observed between the $TiO_{0.89}N_{0.71}$ and $TiO_{1.27}N_{0.49}$ films which was assign to changes in phase constituting the film from the NaCl–B1 TiN structure to the r-Ti_2O_3 structure. The diffraction peak at ~ 38° shifts toward higher angles when the oxygen content increasing, hence a general trend of decrease of the cell parameter along the growth direction is observed. The variation of cell parameter the NaCl–B1 TiN structure between the film $TiO_{0.63}N_{0.96}$ and $TiO_{0.89}N_{0.71}$ was estimated from a = 4.205(5) Å to a = 4.193(5) Å. The variation of out of plane cell parameter of the rhombohedral Ti_2O_3 structure between the film $TiO_{1.27}N_{0.49}$ and
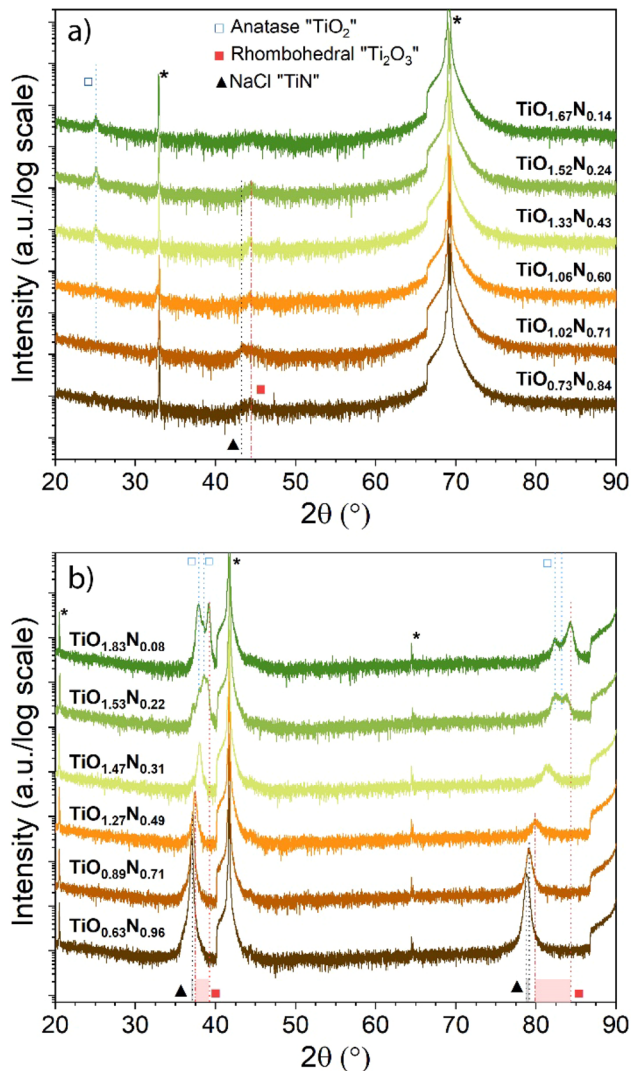
Figure 1 X-ray diffraction patterns of Ti(O,N) thin films deposited on **a** silicon wafer and **b** c-plane sapphire substrates at different O/N flow rates.

$TiO_{1.83}N_{0.08}$ is estimated from c = 14.415(5) Å to c = 13.790(5) Å. Note that the presence of the $r\text{-}Ti_2O_3$ phase was not entirely excluded for the film $TiO_{0.63}N_{0.96}$ and $TiO_{0.89}N_{0.71}$ due to possible overlapping.

$TiO_{1.53}N_{0.22}$ and $TiO_{1.83}N_{0.08}$ films present more complex XRD patterns with the presence of several peaks $\sim 39°$ and $\sim 84°$. The detected peaks were identified as (i) $a\text{-}TiO_2$ (anatase) with a = 3.896 Å and c = 9.36 Å cell parameters (ii) a $r\text{-}Ti_2O_3$ with peaks at higher 2θ angle. This variation of phases was consistent with the elemental composition and ratio Ti/(O + N) closer to $r\text{-}Ti_2O_3$ at high nitrogen content while closer to $a\text{-}TiO_2$ for high oxygen content film (Table 2). Similar investigation on TiO_xN_y thin films

have shown that the films deposited at 500 °C or above were composed of a mixture of NaCl type $TiN_{1-x}O_x$ and anatase TiO_2 while being amorphous when grown at lower temperature [3, 31]. As shown in Fig. 2, at high oxygen content, e.g., $TiO_{1.53}N_{0.22}$ and $TiO_{1.83}N_{0.08}$ films were comprised of a mixture of $r\text{-}Ti_2O_3$, in which the nitrogen could be inserted in anion lattice sites $(r\text{-}Ti_2(O_{1y}N_y)_3)$, and an $a\text{-}TiO_2$ phases.

Figure 2 presents Ti 2p, O 1 s, N 1 s, and C 1 s core levels XPS spectra of Ti(O,N) thin films deposited on silicon wafer and sapphire substrates at room temperature. Although the composition of the same film on different substrates varied to some extent within measurement uncertainty the XPS showed similar trend versus the O/N content in the film. The intensity of the N 1 s decreased while the one from O 1 s intensity increased. The latter was in good agreement with variation of reactive gas flow ratio presented Table 1. For the N 1 s spectra in Fig. 2 c) and f), the position of the N 1 s peak of NaCl TiN and NaCl TiO_xN_y were used as reference [41]. For the O 1 s spectra (Fig. 2 b) and e)), three peak positions were used as reference: $a\text{-}TiO_2$ (530.0 eV), $r\text{-}Ti_2O_3$ (531.1 eV) and in NaCl B1 TiO_xN_y (531.9 eV) [41]. An increase of oxygen content yielded a variation of the peak shape where contribution of several peaks could be expected ($a\text{-}TiO_2$, $r\text{-}Ti_2O_3$ and NaCl B1 TiO_xN_y). At higher oxygen content, components at lower binding energy were becoming predominant.

The progressive introduction of oxygen into the film modified the Ti 2p spectra indicating changes in the chemical bonding of the film. Reference peaks for Ti $2p_{3/2}$ were used in Fig. 1a): 455.2 eV for TiN and its satellite; 456.2 eV for TiO_xN_y; 458.1 eV for Ti_2O_3, and 459.2 eV for TiO_2 [31, 41–43]. The intensity of each component in the Ti 2p peak gradually varied with the oxygen content. For the film having the least amount of oxygen, the XPS spectra of Ti 2p seemed to be composed of a single contribution with a peak position close to TiN (455.2 eV) and its satellite (457.5 eV). When the oxygen increased in the films, the intensity of the nitride component reduced with the emergence of other components at higher binding energy such as oxide (Ti_2O_3 or TiO_2) component. These observations revealed a possible multiphase character of the films where several phases with different crystal structures could be expected when the oxygen content was higher in the series. On both substrates, the XPS spectra peak revealed the change
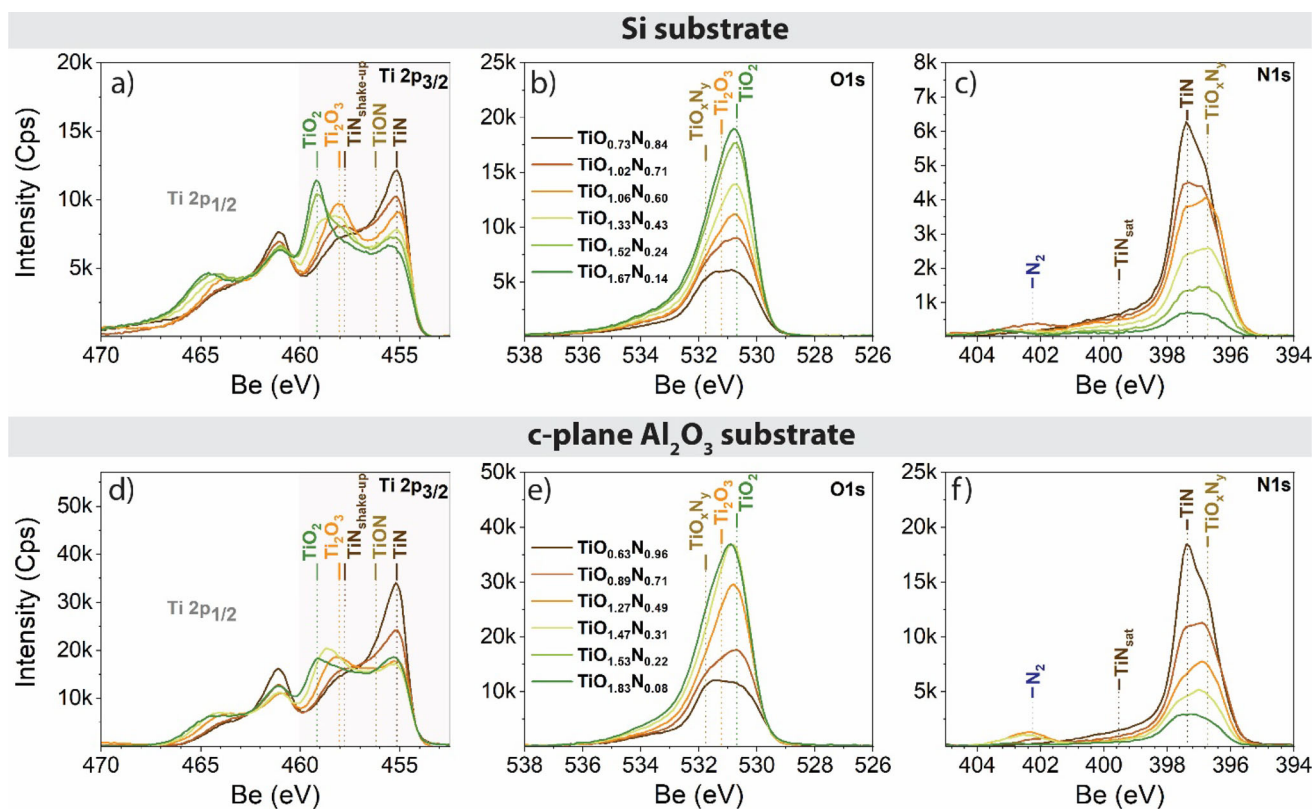
Figure 2 XPS spectra of Ti 2p, N 1 s and O 1 s core-level signals from Ti(O,N) thin films deposited on **a, b, c** silicon substrate and on **d, e** and **f** c-plane sapphire substrate.

of Ti environment with the more pronounced contribution from oxynitride/oxide than from a nitride component when oxygen content increased in the films.

The XRD results and interpretation were in consistency with the XPS results revealing the possible presence of several phases for which possible partial substitution in the anionic network: (i) a NaCl structure $TiN_{1-x}O_x$ for the nitrogen-rich containing films, (ii) $r-Ti_2(O_{1-y}N_y)_3$ for the intermediate N/O ratios, and a mixture of $a-Ti(O_{1-z}N_z)_2$ and $r-Ti_2(O_{1-y}N_y)_3$ structures for films with the highest oxygen content.

Figure 3 shows the surface morphology of the Ti(O,N) thin films deposited on Si and c-plane sapphire substrates with different O/N ratios. The film thickness decreased from 80 to 55 nm when the oxygen content in the films increased. Poisoning of the titanium target during the process when adding oxygen in the plasma was responsible for the thickness decrease. The films could be divided into subgroups depending on the used substrate. $TiO_{0.73}N_{0.84}$ and $TiO_{1.02}N_{0.71}$ films with high N content on Si

substrate show homogeneous nanocrystalline grains. When the oxygen content increased in the films, c.f. $TiO_{1.06}N_{0.60}$ and $TiO_{1.33}N_{0.43}$, another type of grain emerged with a larger grain size indicating the possible presence of two phases in the films. Finally, $TiO_{1.52}N_{0.24}$ and $TiO_{1.67}N_{0.14}$ films had homogeneous morphology with elongated nanocrystalline grains and locally bigger grains.

On c-plane sapphire, the four highest containing nitrogen films have similar morphology with dense smooth nanocrystalline morphology. The two highest oxygen containing films have a different morphology, similarly as the highest containing film on Si, with elongated nanocrystalline grains. Note here, on the films $TiO_{1.47}N_{0.31}$, locally some elongated nanograins were observed. The variation of morphology observed by SEM was following the changes and corresponds to variations of phases constituting the film which have different structure and symmetry (cubic, rhombohedral, tetragonal). When increasing the oxygen in a TiO_xN_{1-x}, Grains sizes varies for $TiO_{1.27}N_{0.49}$ film when the $r-Ti_2O_3$ structure appears;
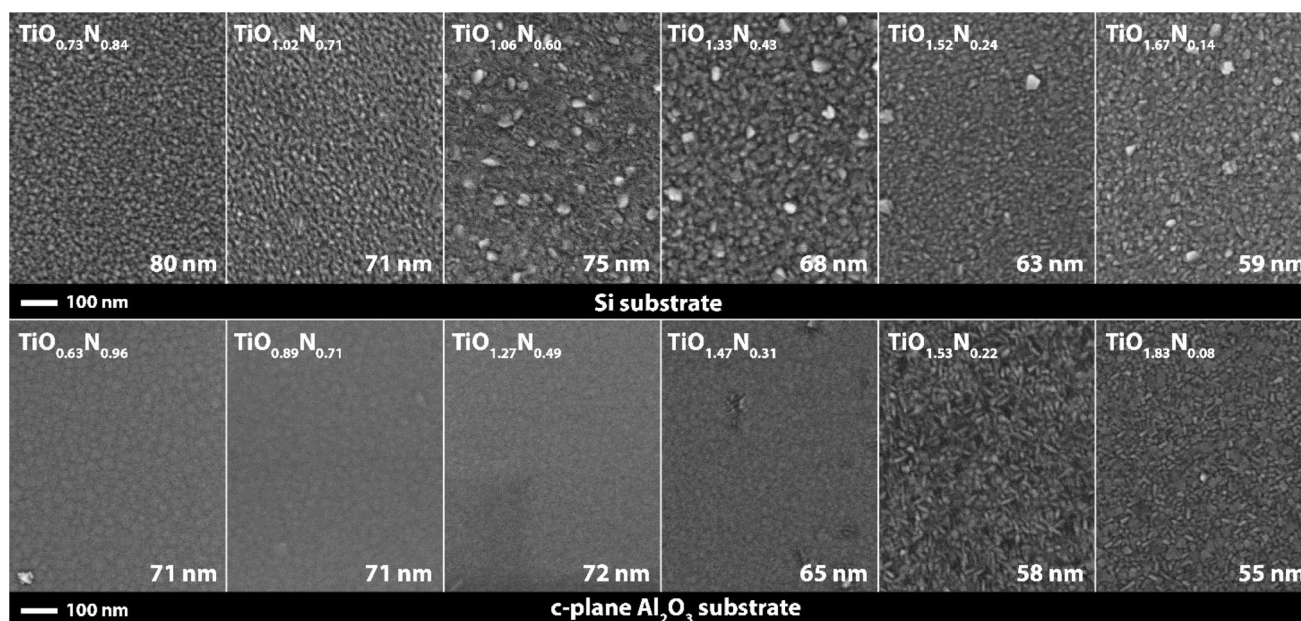
Figure 3 SEM surface micrographs of the Ti(O,N) thin films prepared in various O/N ratio. The thickness determined by ellipsometry is mentioned for each film.

or for the $TiO_{1.55}N_{0.22}$ film when the a-TiO_2 structure phase emerged.

Figure 4 shows the refractive index, extinction coefficient, and absorption coefficient of Ti(O,N) thin films deposited on Si and c-plane sapphire substrates. More details about the variation of optically graded films can be found in Figure S1 in the supplementary information. The graded refractive index detected on some film was believed to be caused by a columnar growth as commonly observed on columnar films [44, 45]. The values of the refractive index reported in Fig. 4 are the values extracted at the bottom of the film. Those values are the most representative and presented for all samples in the series.

The complex refractive index as a function of wavelength, as well as the absorption coefficient as a function of energy, and a clear trend can be seen where higher absorption at longer wavelengths corresponds to films with a higher N-content. As a general trend here, Similarities and subgrouping were observed within the sample series in a similar way as it was observed by XRD, SEM and XPS.

On Si substrate, $TiO_{0.73}N_{0.84}$ and $TiO_{1.02}N_{0.71}$ films (subgroup g1) exhibited a lower refractive index with a pronounced feature around 405 nm. $TiO_{1.52}N_{0.24}$ and $TiO_{1.67}N_{0.14}$ films (subgroup g3) exhibited a significantly sharper feature at around 320 nm, and

$TiO_{1.06}N_{0.60}$ and $TiO_{1.33}N_{0.43}$ films (subgroup g2) exhibited a mix of both these features.

According to XRD patterns of the films on both substrates, the films with higher oxygen content contained a mixture a-TiO_2 and r-Ti_2O_3 phases, the samples with higher nitrogen content contained a NaCl B1 TiN structure, while the intermediate composition were composed mainly of Ti_2O_3.

The absorption coefficient, being related to the refractive index, (Fig. 4c) revealed an absorption in the entire investigated spectrum for samples $TiO_{0.73}N_{0.84}$ and $TiO_{1.02}N_{0.71}$, whereas the rest of the samples grown on Si substrates exhibited a section of the spectrum with zero, or nearly zero absorption (α). The onset of absorption shifted towards higher energy/shorter wavelengths with decreasing N-content. The two samples e.g., $TiO_{0.73}N_{0.84}$, and $TiO_{1.02}N_{0.71}$ (subgroup g1), exhibited metallic properties, which was why the optical model for those films contained Drude-oscillator components [29].

The samples grown on sapphire substrates could be divided into three subgroups, where $TiO_{1.53}N_{0.22}$ and $TiO_{1.83}N_{0.08}$ films (subgroup g6) exhibited one relatively sharp feature in refractive index at around 320 nm whereas $TiO_{0.63}N_{0.96}$, $TiO_{0.89}N_{0.71}$, $TiO_{1.27}N_{0.49}$, and $TiO_{1.27}N_{0.49}$ films (subgroup g4 and g5) exhibited significantly broader features centered at longer wavelengths/lower energies. Only the films
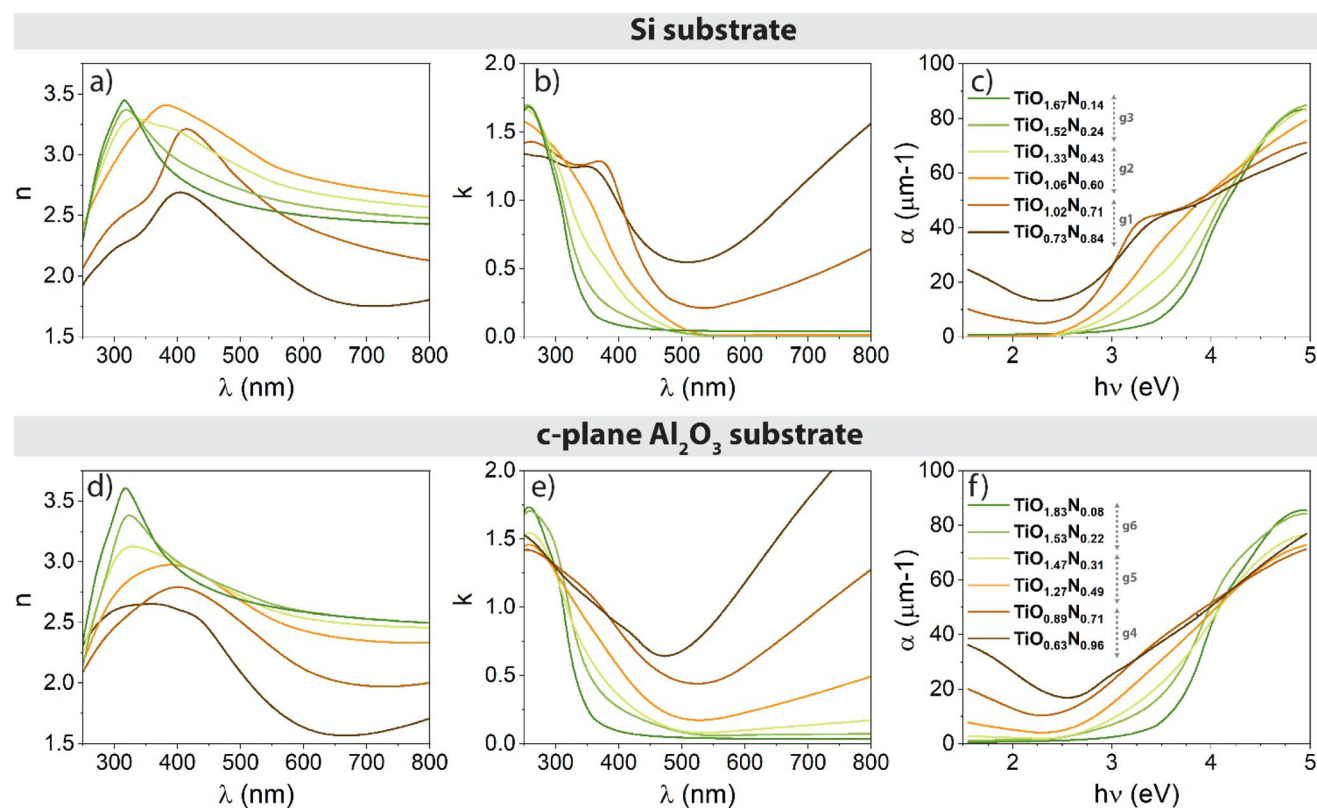
Figure 4 Refractive index, extinction coefficient, absorption coefficient, respectively of the Ti(O,N) thin films prepared in various O/N ratio on **a, b, c** Si substrates and **d, e, f** on sapphire substrate.

belonging to subgroup (g6) exhibit spectral regions with zero absorption. Moreover, a metallic behavior was observed when the N-content increases, and in this case three of the samples ($TiO_{0.73}N_{0.84}$, $TiO_{1.02}N_{0.71}$, and $TiO_{0.63}N_{0.96}$) were modelled using Drude oscillators. A fourth sample ($TiO_{0.89}N_{0.71}$) exhibited a tendency towards metallic absorption, however too small to be modelled with a Drude oscillator model.

Where applicable, bandgap values have been calculated using a modified Cody plot [30], and the values can be found in table S1 and Figure S2. All bandgap values are decreasing with increased nitrogen from a maximum recorded of 3.75 eV, which is somewhat higher than the value for pure a-TiO_2 reported elsewhere[46] (3.2 eV). The difference in band gap energies recorded on the films containing the higher amount of oxygen could be attributed to the non-single phase containing aspect of the film and the partial substitution in the anionic network.

From the most oxidized coating, insertion of nitrogen in the film yielded a decrease of the band gap from 3.75 eV ($TiO_{1.67}N_{0.14}$) to 3.00 eV($TiO_{1.06}N_{0.60}$) on Si (100) and from 3.75 eV ($TiO_{1.83}N_{0.08}$) to 3.50 eV($TiO_{1.47}N_{0.31}$). Substitution in As the substitutional atom, the nitrogen in an oxygen site would act

as a donor, resulting in an increase of the band gap with hybridization of the N 2p and O 2p lowering the valence band towards the conduction band (composed mainly by the 3d orbitals of the metal) [5, 38, 47]. When nitrogen atoms are incorporated in the crystal lattice of either anatase TiO_2 or r-Ti_2O_3, the valence band is lowered hence the bandgap is reduced of the material. As a result, photons with lower energies, including those in the visible light range, can now be absorbed by the material, hence reduces the transparency of the material to visible light [48]. This study shows that the effect of nitrogen substitution in anatase TiO_2 and the r-Ti_2O_3 present similitudes for which growth competition seemed to occur at specific composition in the nitrogen/oxygen composition spectrum of the materials system Ti(O,N) grown in those deposition conditions.

Conclusions

TiO_xN_y films, with $0.63 < x < 1.83$ and $0.96 > y > 0.08$, were deposited on Si and c-plane Al_2O_3 substrates by reactive RF magnetron sputtering in a UHV deposition system. Crystalline thin films

were grown, and the phase composition of the films varied depending on the O/N content. The N-rich films ($x < 0.9$ and $y > 0.7$) were composed of a NaCl B1 $TiN_{1-x}O_x$ phase, while the O-rich films ($x > 1.5$ and $y < 0.2$) were composed of the anatase $Ti(O_{1-z}N_z)_2$ and rhombohedral phase. The films with intermediate compositions were constituted of the r-$Ti_2(O_{1-y}N_y)_3$ phase. The variation of phases combined with possible substitution in the anionic network of the three phases NaClB1 TiN, r-Ti_2O_3, a-TiO_2 influences the optical properties of the obtained films. The optical properties measured by spectroscopic ellipsometry revealed a shift in the absorption edge of the film towards longer wavelengths for films with a higher N-content. The band gap values increased from 3.0 to 3.7 eV, making the material more transparent upon increase of O-content. On the increase of nitrogen, the film exhibited metallic properties, with absorption in the entire UV–VIS-NIR spectral region.

Acknowledgements

Funding

Data availability

Not applicable.

Declarations

Conflict of interest The authors declare no competing financial interest.

Ethical approval Not applicable.

Supplementary Information: The online version contains supplementary material available at https://doi.org/10.1007/s10853-023-08717-8.

References

[1] Guillot J, Fabreguette F, Imhoff L, Heintz O, Marco de Lucas MC, Sacilotti M, Domenichini B, Bourgeois S (2001) Amorphous TiO2 in LP-OMCVD TiNxOy thin films revealed by XPS. Appl Surf Sci 177(4):268–272

[2] Chappé J-M, Martin N, Terwagne G, Lintymer J, Gavoille J, Takadoum J (2003) Water as reactive gas to prepare titanium oxynitride thin films by reactive sputtering. Thin Solid Films 440(1):66–73

[3] Mucha NR, Som J, Shaji S, Fialkova S, Apte PR, Balasubramanian B, Shield JE, Anderson M, Kumar D (2020) Electrical and optical properties of titanium oxynitride thin films. J Mater Sci 55(12):5123–5134

[4] Braic M, Balaceanu M, Vladescu A, Kiss A, Braic V, Epurescu G, Dinescu G, Moldovan A, Birjega R, Dinescu M (2007) Preparation and characterization of titanium oxy-nitride thin films. Appl Surf Sci 253(19):8210–8214

[5] Aoki Y, Sakurai M, Coh S, Chelikowsky JR, Louie SG, Cohen ML, Saito S (2019) Insulating titanium oxynitride for visible light photocatalysis. Phys Rev B 99(7):075203

[6] Cuong ND, Kim D-J, Kang B-D, Yoon S-G (2006) Structural and Electrical properties of TiN_xO_y thin-film resistors for 30 dB applications of π-type attenuator. J Electrochem Soc 153(9):G856

[7] Koerner RJ, Butterworth LA, Mayer IV, Dasbach R, Busscher HJ (2002) Bacterial adhesion to titanium-oxy-nitride

(TiNOX) coatings with different resistivities: a novel approach for the development of biomaterials. Biomaterials 23(14):2835–2840

[8] Chen F, Wang S-W, Yu L, Chen X, Lu W (2014) Control of optical properties of TiNxOy films and application for high performance solar selective absorbing coatings. Opt Mater Express 4(9):1833–1847

[9] Cristea D, Velicu I-L, Cunha L, Barradas N, Alves E, Craciun V (2022) Tantalum-titanium oxynitride thin films deposited by DC reactive magnetron co-sputtering: mechanical, optical, and electrical characterization. Coatings 12(1):36

[10] Stranak V, Quaas M, Bogdanowicz R, Steffen H, Wulff H, Hubicka Z, Tichy M, Hippler R (2010) Effect of nitrogen doping on TiOxNy thin film formation at reactive high-power pulsed magnetron sputtering. J Phys D Appl Phys 43(28):285203

[11] Akazawa H (2012) Sputtering characteristics, crystal structures, and transparent conductive properties of TiOxNy films deposited on α-Al$_2$O$_3$(0001) and glass substrates. Appl Surf Sci 263:307–313

[12] Wu PG, Ma CH, Shang JK (2005) Effects of nitrogen doping on optical properties of TiO$_2$ thin films. Appl Phys A 81(7):1411–1417

[13] Martev IN (2002) XRD and AES characterization of TiOxNy thin films grown by ion assisted deposition. Vacuum 67(2):261–265

[14] Song X, Gopireddy D, Takoudis CG (2008) Characterization of titanium oxynitride films deposited by low pressure chemical vapor deposition using amide Ti precursor. Thin Solid Films 516(18):6330–6335

[15] Yu YP, Liu W, Wu SX, Li SW (2012) Impact of nitrogen doping on electrical conduction in anatase TiO$_2$ thin films. J Phys Chem C 116(37):19625–19629

[16] Granier B, Renard R, Coutures JP (1980) Ternary phase diagram of Ti–O–N: study of the TiO–TiN cubic solid solution. Revue internationale des hautes températures et des réfractaires 17(3):235–247

[17] Martin N, Banakh O, Santo AME, Springer S, Sanjinés R, Takadoum J, Lévy F (2001) Correlation between processing and properties of TiOxNy thin films sputter deposited by the reactive gas pulsing technique. Appl Surf Sci 185(1):123–133

[18] Akazawa H (2022) Transparent conductive properties of TiON thin films. J Vac Sci Technol A 40(1):013407

[19] Graciani J, Hamad S, Sanz JF (2009) Changing the physical and chemical properties of titanium oxynitrides TiN$_{1-x}$O$_x$ by changing the composition. Phys Rev B 80(18):184112

[20] Vaz F, Cerqueira P, Rebouta L, Nascimento SMC, Alves E, Goudeau P, Rivière JP, Pischow K, de Rijk J (2004) Structural, optical and mechanical properties of coloured TiNxOy thin films. Thin Solid Films 447–448:449–454

[21] Syono Y, Goto T, Nakai J, Nakagawa Y, Iwasaki H (1974) Shock compression of titanium monoxide up to 600 kbar. J Phys Soc Jpn 37(2):442–446

[22] Sharan A, Lany S (2021) Computational discovery of stable and metastable ternary oxynitrides. J Chem Phys 154(23):234706

[23] Graciani J, Sanz JF, Asaki T, Nakamura K, Rodriguez JA (2007) Interaction of oxygen with TiN(001):N↔O exchange and oxidation process. J Chem Phys 126(24):244713

[24] le Febvrier A, Landälv L, Liersch T, Sandmark D, Sandström P, Eklund P (2021) An upgraded ultra-high vacuum magnetron-sputtering system for high-versatility and software-controlled deposition. Vacuum 187:110137

[25] Shirley DA (1972) High-resolution X-ray photoemission spectrum of valence bands of gold. Phys Rev B 5(12):4709–5000

[26] Haasch RT, Lee T-Y, Gall D, Greene JE, Petrov I (2000) Epitaxial TiN(001) grown and analyzed in situ by XPS and UPS. II. analysis of Ar+ sputter etched layers. Surf Sci Spectra 7(3):204–212

[27] Seah MP (2001) Summary of ISO/TC 201 standard: VII ISO 15472: 2001—surface chemical analysis—x-ray photoelectron spectrometers—calibration of energy scales. Surf Interface Anal 31(8):721–723

[28] Greczynski G, Hultman L (2020) X-ray photoelectron spectroscopy: towards reliable binding energy referencing. Prog Mater Sci 107:100591

[29] Ferlauto AS, Ferreira GM, Pearce JM, Wronski CR, Collins RW, Deng X, Ganguly G (2002) Analytical model for the optical functions of amorphous semiconductors from the near-infrared to ultraviolet: applications in thin film photovoltaics. J Appl Phys 92(5):2424–2436

[30] Bairagi S, Hsiao C-L, Magnusson R, Birch J, Chu JP, Tarntair F-G, Horng R-H, Järrendahl K (2022) Zinc gallate (ZnGa2O4) epitaxial thin films: determination of optical properties and bandgap estimation using spectroscopic ellipsometry. Opt Mater Express 12(8):3284–3295

[31] Banakh O, Moussa M, Matthey J, Pontearso A, Cattani-Lorente M, Sanjines R, Fontana P, Wiskott A, Durual S (2014) Sputtered titanium oxynitride coatings for endosseous applications: physical and chemical evaluation and first bioactivity assays. Appl Surf Sci 317:986–993

[32] Vaz F, Carvalho P, Cunha L, Rebouta L, Moura C, Alves E, Ramos AR, Cavaleiro A, Goudeau P, Rivière JP (2004) Property change in ZrNxOy thin films: effect of the oxygen fraction and bias voltage. Thin Solid Films 469–470:11–17

[33] Ali S, Paul B, Magnusson R, Broitman E, Jonson B, Eklund P, Birch J (2017) Synthesis and characterization of the

mechanical and optical properties of Ca–Si–O–N thin films deposited by RF magnetron sputtering. Surf Coat Technol 315:88–94

[34] Ali S, Paul B, Magnusson R, Ekström E, Pallier C, Jonson B, Eklund P, Birch J (2019) Optical and mechanical properties of amorphous Mg–Si–O–N thin films deposited by reactive magnetron sputtering. Surf Coat Technol 372:9–15

[35] Hakeem AS, Dauce R, Leonova E, Edén M, Shen ZJ, Grins J, Esmaeilzadeh S (2005) Silicate glasses with unprecedented high nitrogen and electropositive metal contents obtained by using metals as precursors. Adv Mater 17(18):2214–2216

[36] Genson A, Hanifi AR, Put AV, Pomeroy MJ, Hampshire S (2007) Effect of fluorine and nitrogen anions on properties of Ca–Si–Al–O glasses. Mater Sci Forum 554:31–35

[37] Sharafat A, Forslund B, Grins J, Esmaeilzadeh S (2009) Formation and properties of nitrogen-rich strontium silicon oxynitride glasses. J Mater Sci 44(2):664–670

[38] Mucha NR, Som J, Choi J, Shaji S, Gupta RK, Meyer HM, Cramer CL, Elliott AM, Kumar D (2020) High-performance titanium oxynitride thin films for electrocatalytic water oxidation. ACS Appl Energy Mater 3(9):8366–8374

[39] Ney A, Rajaram R, Parkin SSP, Kammermeier T, Dhar S (2006) Magnetic properties of epitaxial CrN films. Appl Phys Lett 89(11):112504

[40] Talyansky V, Choopun S, Downes MJ, Sharma RP, Venkatesan T, Li YX, Salamanca-Riba LG, Wood MC, Lareau RT, Jones KA (1999) Pulsed laser deposition of titanium nitride films on sapphire. J Mater Res 14(8):3298–3302

[41] NIST X-ray Photoelectron Spectroscopy Database, N. S. R. D. N., (2000) National Institute of Standards and Technology, Gaithersburg MD, 20899. Accessed 26 Dec 2022

[42] Saha NC, Tompkins HG (1992) Titanium nitride oxidation chemistry: an x-ray photoelectron spectroscopy study. J Appl Phys 72(7):3072–3079

[43] Chan M-H, Lu F-H (2009) X-ray photoelectron spectroscopy analyses of titanium oxynitride films prepared by magnetron sputtering using air/Ar mixtures. Thin Solid Films 517(17):5006–5009

[44] Szczyrbowski J, Bräuer G, Ruske M, Bartella J, Schroeder J, Zmelty A (1999) Some properties of TiO2 layers prepared by medium frequency reactive sputtering. Surf Coat Technol 112(1):261–266

[45] Le Febvrier A, Galca AC, Corredores Y, Députier S, Bouquet V, Demange V, Castel X, Sauleau R, Lefort R, Zhang LY, Tanné G, Pintilie L, Guilloux-Viry M (2012) Structural, optical, and dielectric properties of Bi1.5–xZn0.92–yNb1.5O6.92−δ thin films grown by PLD on R-plane sapphire and LaAlO3 substrates. ACS Appl Mater Interfaces 4(10):5227–5233

[46] Dette C, Pérez-Osorio MA, Kley CS, Punke P, Patrick CE, Jacobson P, Giustino F, Jung SJ, Kern K (2014) TiO$_2$ anatase with a bandgap in the visible region. Nano Lett 14(11):6533–6538

[47] Ahmed M, Xinxin G (2016) A review of metal oxynitrides for photocatalysis. Inorg Chem Front 3(5):578–590

[48] Naveen Kumar SY, Mittal A, Kumari K (2021) Photocatalysis by zinc oxide-based nanomaterials. Nanostructured Zinc Oxide Synthesis, Properties and Applications Metal Oxides. Elsevier, pp 393–457